Effect of chemical and hydrostatic pressure on the cubic pyrochlore $Cd_2Ru_2O_7$

Y. Y. Jiao,[1,2] J. P. Sun,[1,2] P. Shahi,[1,2] Q. Cui,[1,2] X. H. Yu,[1,2] Y. Uwatoko,[3] B. S. Wang,[1,2] J. A. Alonso,[4] H. M. Weng,[1,2] and J.-G. Cheng[1,2,*]

[1]*Beijing National Laboratory for Condensed Matter Physics and Institute of Physics, Chinese Academy of Sciences, Beijing 100190, China*
[2]*School of Physical Sciences, University of Chinese Academy of Sciences, Beijing 100190, China*
[3]*Institute for Solid State Physics, University of Tokyo, 5-1-5 Kashiwanoha, Kashiwa, Chiba 277-8581, Japan*
[4]*Instituto de Ciencia de Materiales de Madrid, CSIC, Cantoblanco, E-28049 Madrid, Spain*

(Received 12 February 2018; revised manuscript received 26 July 2018; published 8 August 2018)

The cubic pyrochlore $Cd_2Ru_2O_7$ develops a metalliclike state below the antiferromagnetic transition at $T_N \approx 90$ K, in contrast to the sharp transition to an insulating state below T_N of the 5*d*-analog $Cd_2Os_2O_7$. We have synthesized polycrystalline $Cd_2Ru_2O_7$ under high pressure, and investigated the responses of its electronic behavior to hydrostatic pressure and isovalent substitutions of Ca^{2+} for Cd^{2+}. Three characteristic anomalies are identified in the electrical transport and magnetic properties of $Cd_2Ru_2O_7$, signaling an intimate correlation between charge and spin degrees of freedom. Interestingly, we found that the metalliclike state of $Cd_2Ru_2O_7$ below T_N is very fragile and can be suppressed by a small hydrostatic pressure of $\leqslant 1$ GPa or substitution of 5–10% Ca^{2+} for Cd^{2+}, resulting in a resistivity behavior similar to that of $Cd_2Os_2O_7$. In addition, the resultant insulating state below T_N is very robust against pressure, and the resistivity evolves gradually into two distinct activated regions under higher pressures. We constructed a temperature-pressure phase diagram for $Cd_2Ru_2O_7$ and discussed its peculiar metalliclike state in terms of the electronic itinerancy/localization dichotomy via side-by-side comparisons with the related compounds $A_2Ru_2O_7 (A = \text{Ca, Hg})$ and $Cd_2Os_2O_7$. Our results demonstrate that these cubic $4d/5d$ pyrochlore oxides offer an important paradigm for studying the exotic physics of correlated electrons on the border of (de)localization in the presence of strong geometrical frustration.

DOI: 10.1103/PhysRevB.98.075118

I. INTRODUCTION

One challenging problem in strongly correlated electron systems is to understand the electronic behaviors near the localized to itinerant crossover, which lie at the heart of many exotic phenomena such as unconventional superconductivity, metal-insulator transition, and quantum criticality [1–3]. The Ru^{5+} pyrochlore oxides $A_2Ru_2O_7 (A = \text{Ca, Cd, Hg})$ [4–7] with a divalent A^{2+} cation comprise such a system in which the Ru $4d$ electrons acquire the characteristics of both itinerancy and localization [8]. In particular, the magnetic Ru^{5+} ($4d^3$) ions that are situated on the vertices of a corner-shared tetrahedral lattice are subjected to strong geometrical frustration for antiferromagnetic (AF) interactions [8,9]. As such, the presence of both electronic dichotomy and strong geometrical frustration in these Ru^{5+}-pyrochlore oxides produces distinct ground states, which were found to vary sensitively as a function of the *A*-cation covalency on the order of Ca < Cd < Hg [8].

For $Ca_2Ru_2O_7$ with more ionic Ca^{2+}, it forms a spin-glass magnetic state below $T_f \approx 23$ K, as exemplified by the bifurcation of field-cooled (FC) and zero-field-cooled (ZFC) magnetic susceptibility [4,10]. The effective magnetic moment of $\sim 0.36\mu_B/Ru^{5+}$ extracted from the Curie-Weiss fitting is one order lower than the expected value for localized $S = 3/2$. Although its resistivity in the whole temperature range takes relatively low values of 2–4 mΩ cm typical for correlated metallic oxides, the observed semiconducting-like temperature dependence, $d\rho/dT < 0$, is contrary to a simple metallic behavior. No discernable anomaly was observed around T_f in resistivity. Muon-spin rotation (μSR) measurements have confirmed the presence of highly inhomogeneous local magnetism below T_f [8]. The observation of bad metallic behavior with a concurrent spin-frozen state in single-phase $Ca_2Ru_2O_7$ thus demonstrates an intrinsic dichotomy of Ru $4d$ electrons in a typical geometrically frustrated lattice.

When the *A* site is occupied by more covalent Hg^{2+}, $Hg_2Ru_2O_7$ displays a metallic behavior, i.e., $d\rho/dT > 0$, around room temperature, and it undergoes a sharp metal-to-insulator transition at $T_N = 107$ K [6,7], which is accompanied by a long-range AF order and a first-order structural transition from cubic to monoclinic symmetry [11]. The low-temperature monoclinic structure has been determined as a stacking of kagome-like layers associated with a splitting of the Ru-Ru bond lengths, rendering more two-dimensional exchange interactions between the Ru ions [11]. The MIT was proposed to be a self-doping induced orbital-selective Mott transition, or to result from covalency-driven charge disproportionation [12,13].

For $Cd_2Ru_2O_7$ with intermediate *A*-O covalency, no structural transition was observed around $T_N \approx 100$ K [5]. Its magnetic susceptibility displays a drop at T_N similar to that of $Hg_2Ru_2O_7$, while the resistivity undergoes a gradual decrease and exhibits a metalliclike temperature dependence in the temperature range 60–100 K [6,7]. Such an AF metallic ground

*jgcheng@iphy.ac.cn

state is rarely seen among the single-valent transition-metal oxides. For example, the $5d$-analog $Cd_2Os_2O_7$ displays a continuous metal-to-insulator transition upon the development of AF order around $T_N = 225$ K [14]. More interestingly, recent first-principles calculations by Weng *et al.* have predicted multiple topological phase transitions induced by the "all-in, all-out" (AIAO) type AF order in $Cd_2Ru_2O_7$; the metalliclike state just below T_N was ascribed to a Weyl semimetallic state due to the breaking of time-reversal symmetry [15]. Despite these unusual physical properties and potential topological states in $Cd_2Ru_2O_7$, only a few experimental studies have been performed on this interesting compound so far, presumably due to difficulties in stabilizing the high oxidation state of Ru^{5+} [5].

To obtain a deeper understanding of the electronic behaviors of $Cd_2Ru_2O_7$, especially on the peculiar metalliclike state just below T_N, we performed a comprehensive study on the responses of its electronic behavior to external hydrostatic pressure and isovalent chemical substitutions of Ca^{2+} for Cd^{2+} on polycrystalline samples synthesized under high oxygen pressure. We found that the metalliclike state of $Cd_2Ru_2O_7$ below T_N is very fragile and can be readily converted to an insulting phase by applying ~1 GPa hydrostatic pressure or replacing 5–10 % Cd^{2+} with Ca^{2+}. The resultant resistivity behavior is similar to that of $Cd_2Os_2O_7$. In addition, the insulating state is very robust against pressure, and the resistivity evolves gradually into two distinct activated regions under higher pressures. We have discussed the peculiar metalliclike state and its unusual responses to perturbations in terms of electronic dichotomy via side-by-side comparisons with the related compounds $A_2Ru_2O_7 (A = Ca, Hg)$ and $Cd_2Os_2O_7$. Our results demonstrate that $Cd_2Ru_2O_7$ and related $4d/5d$ cubic pyrochlore oxides offer an important paradigm for studying the exotic physics of correlated electrons on the border of (de)localization in the presence of strong geometrical frustration.

II. EXPERIMENT

All the polycrystalline $Cd_{2-x}Ca_xRu_2O_7 (0 \leqslant x \leqslant 2.0)$ samples used in the present study were prepared under high-pressure and high-temperature (HPHT) conditions with a Kawai-type multianvil module. These samples were obtained by sintering the stoichiometric mixture of CdO, CaO, and RuO_2 mixed with 20–30 wt.% $KClO_4$ in a sealed gold capsule at 4 GPa and 1000 °C for 30 min. Here, the $KClO_4$ was added as the oxygen source to create a high oxygen pressure within the sealed high-pressure compartment so as to stabilize the high oxidation Ru^{5+} state in these samples. The resultant KCl was washed away with the deionized water after synthesis. To obtain dense pellets for various physical-property measurements, we have further treated the obtained powders with $KClO_4$ on both sides of sample under similar HPHT conditions. Details about the sample assembly and the procedure for HPHT synthesis can be found elsewhere [16].

Phase purity of the obtained samples was examined by powder x-ray diffraction (XRD) at room temperature with Cu $K\alpha$ radiation. Structural parameters were extracted from the XRD pattern via Rietveld refinement using the FULLPROF program. DC magnetic susceptibility was measured with a commercial Magnetic Property Measurement System (MPMS-III, Quantum Design) in the temperature range from 2 to 300 K under an external magnetic field of $\mu_0 H = 1$ T. A Physical Property Measurement System (PPMS-9T, Quantum Design) was employed to measure the electrical resistivity with a standard four-probe method and the specific heat with the two-τ relaxation method in the temperature range from 2 to 300 K. A home-made setup was used to measure the thermopower with the steady-state method. X-ray photoemission spectra (XPS) were measured using an ESCALAB 250X spectrometer (Thermo-Fisher Scientific) employing monochromatic Al $K\alpha$ radiation (1486.6 eV) at room temperature. The spectra of the peaks of Ru $3d$ were recorded with an energy step of 0.1 eV. The binding energy (BE) of the XPS is calibrated with respect to the pure bulk Au $4f_{7/2}$(BE = 84.0 eV) and Cu $2p_{3/2}$(BE = 932.7 eV) lines. The BE is referenced to the Fermi level (E_f) calibrated by using pure bulk Ni as $E_f = 0$ eV.

High-pressure synchrotron XRD on $Cd_2Ru_2O_7$ was performed at room temperature with a symmetric diamond anvil cell of 300 μm culet at Beijing Synchrotron Radiation Facility with a wavelength of $\lambda = 0.6199$ Å. Neon gas was used as a pressure-transmitting medium, and the pressure values were calculated using the ruby fluorescence method. The temperature dependence of resistivity $\rho(T)$ under various hydrostatic pressures was measured with a self-clamped piston–cylinder cell (PCC) for $P < 2$ GPa [17] and a palm cubic anvil cell (CAC) in the pressure range $2 \leqslant P \leqslant 15$ GPa [18,19]. The pressure values in PCC was determined by monitoring the superconducting transition temperature of lead, and the pressure in CAC was estimated from the calibration curve based on the characteristic transitions of bismuth and lead at room temperature.

III. RESULTS AND DISCUSSION

A. Physical properties of $Cd_2Ru_2O_7$ at ambient pressure

The XRD pattern shown in Fig. 1 confirms that the obtained $Cd_2Ru_2O_7$ sample is nearly single phase with an ~1.9 wt.%

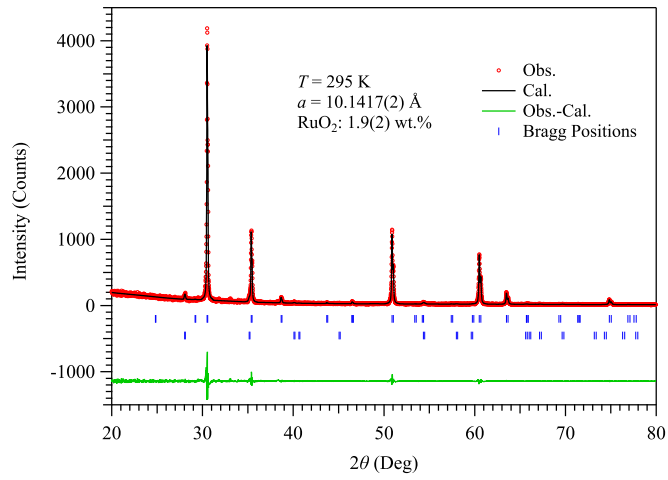

FIG. 1. Rietveld refinement on the XRD pattern of polycrystalline $Cd_2Ru_2O_7$. The top and bottom tick marks correspond to the Bragg positions of the cubic pyrochlore $Cd_2Ru_2O_7$ and the RuO_2 secondary phase, respectively. The obtained lattice constant and the amount of RuO_2 are given in the figure.

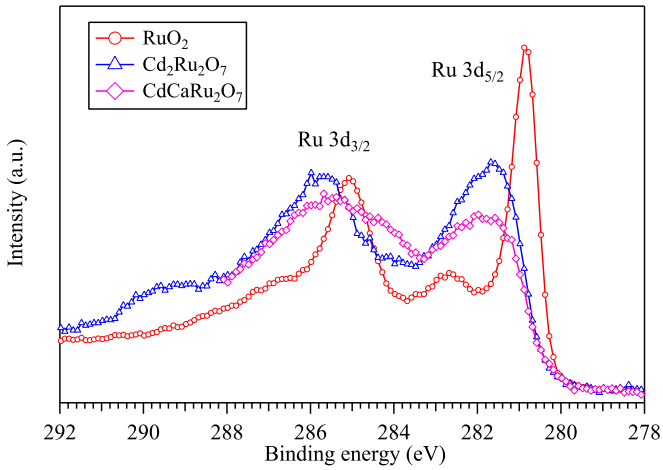

FIG. 2. The XPS of Ru 3*d* for $Cd_2Ru_2O_7$, $CdCaRu_2O_7$, and RuO_2 at room temperature.

RuO_2 impurity. The XRD pattern has been refined with the Rietveld method in a cubic pyrochlore structure with space group $Fd\text{-}3m$ (No. 227) and the Cd atom at $16d(1/2, 1/2, 1/2)$, the Ru atom at $16c(0, 0, 0)$, the O1 at $48f(x, 1/8, 1/8)$, and the O2 at $8b(3/8, 3/8, 3/8)$ site, respectively. The RuO_2 in space group $P4_2/mnm$ (no. 136) was introduced as a secondary phase in the refinement. As illustrated in Fig. 1, the refinement converged well and the obtained lattice constant $a = 10.1417(2)$ Å is slightly larger, but close to the value of 10.129(1) Å for the single-crystal sample reported by Wang and Sleight [5]. The difference $\delta a/a$ is only ~0.125%, and we attributed such a small difference to the different sample preparation conditions as discussed below.

The valence of the Ru ion can be estimated by means of Brown's bond valence model [20,21], which gives a phenomenological relationship between the formal valence of a bond and the corresponding bond length. The valence is the sum of the individual bond valences (s_i) for Ru-O bonds, and the individual bond valence is calculated as $s_i = \exp[(r_0 - r_i)/B]$, in which $B = 0.37$ and $r_0 = 1.900$ for the Ru^{5+}-O^{2-} pair. Based on the obtained Ru-O bond length of 1.932(1) Å from the Rietveld refinements, the bond valence sum (BVS) for Ru is estimated to be +5.5(1), which is larger than the nominal value of +5, presumably due to the uncertainty in determining the oxygen positional parameter x with the laboratory XRD. To further confirm the valence of Ru ions, we measured XPS of $Cd_2Ru_2O_7$ and RuO_2 and compared with that of $Hg_2Ru_2O_7$ [6]. As shown in Fig. 2, the binding energy of the Ru $3d_{5/2}$ peak of $Cd_2Ru_2O_7$ (281.68 eV) is very close to that of $Hg_2Ru_2O_7$ (281.3 eV) [6] and is located 0.8 eV below that of RuO_2 (280.88 eV) with Ru^{4+}. Similar results are also observed in $CdCaRu_2O_7$. These comparisons clearly demonstrate that Ru^{5+} is stabilized in our $Cd_{2-x}Ca_xRu_2O_7$ samples.

Figure 3 summarizes the physical properties of $Cd_2Ru_2O_7$ at ambient pressure. As shown in Fig. 3(a), the temperature dependences of magnetic susceptibility $\chi(T)$ measured under $\mu_0 H = 1$ T exhibit a clear drop around $T_N \approx 85$ K, signaling the occurrence of long-range AF order. It should be noted that the observed T_N in the present study is about 10 K lower than those reported previously [5,8]. As reported by Miyazaki

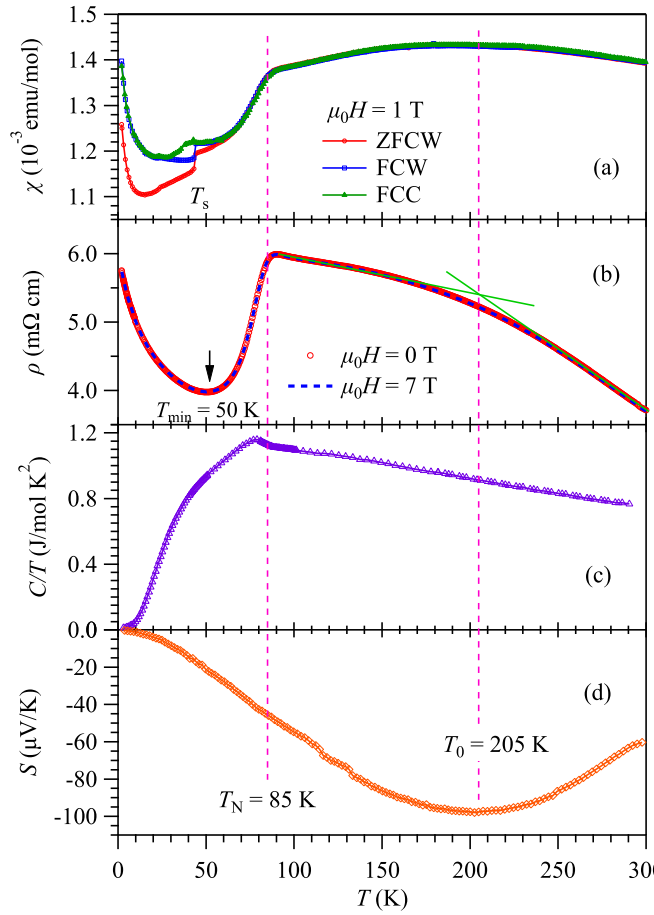

FIG. 3. Temperature dependences of (a) magnetic susceptibility $\chi(T)$ measured under $\mu_0 H = 1$ T, (b) resistivity $\rho(T)$ measured under $\mu_0 H = 0$ and 7 T, (c) specific heat divided by temperature $C/T(T)$, and (d) thermopower $S(T)$ under zero field for the cubic pyrochlore $Cd_2Ru_2O_7$. The antiferromagnetic transition at $T_N = 85$ K together with two other characteristic anomalies at $T_s(T_{min}) \approx 40$–50 K and $T_0 \approx 200$ K for the physical properties are also marked in the figure.

et al. [8], $A_2Ru_2O_7(A = Ca, Cd, Hg)$ samples from different batches show a variation of T_N in the range of 2–5 K. The variation can result from nonstoichiometry, which is determined by the synthesis parameters such as the percentage of oxidizer (e.g., $KClO_4$), the reaction temperature and duration, the sealing condition of the noble-metal capsule, etc. Compared with previous reports, our syntheses were performed at a lower reaction pressure with a shorter duration. Nonetheless, we want to emphasize that the essential features of physical properties shown below are very similar to those reported previously [5,8], including the characteristic drop of $\chi(T)$ and $\rho(T)$ around T_N shown in Fig. 3.

Above T_N, $\chi(T)$ does not follow the Curie-Weiss behavior but displays a broad hump centered around $T_0 \approx 200$ K. Such a feature has also been observed in previous studies [5,8] but received little attention. A similar feature in the paramagnetic magnetic susceptibility was also observed in the *A*-site ordered perovskite $CaCu_3Ru_4O_{12}$ [22], implying the presence of enhanced spin fluctuations. In addition, a sudden drop of $\chi(T)$ at $T_s \approx 40$ K implies the presence of another magnetic

transition within the antiferromagnetically ordered state. This transition has been reported by Miyazaki *et al.* [8] and was attributed to the reduction of Ru magnetic moment in light of the μSR measurements. Interestingly, our measurements of $\chi(T)$ curves in the thermal cycling evidenced a clear hysteresis around T_s, pointing to a first-order nature of this transition. Moreover, a tiny kink anomaly around 25 K can be also discerned in the $\chi(T)$ curves. Given the similar feature to the anomaly around T_s, the weak kink around 25 K might have a common origin due to the reduction of a portion of Ru magnetic moments. The upturn of $\chi(T)$ below 10 K should be attributed to some isolated magnetic impurities such as defects, vacancies, impurities, etc. To estimate the concentration of magnetic impurities, we have fitted the low-temperature tail of $\chi(T)_{FCW}$ in the temperature range 2–12 K with the modified Curie-Weiss law, i.e., $\chi = \chi_0 + C/(T + \theta_{CW})$, and the obtained effective moment $\mu_{eff} = (8C)^{1/2} = 0.10\mu_B$. Assuming the magnetic impurities with a local spin $S = 1/2$, the concentration of impurity can be estimated as 0.34%.

Figure 3(b) shows the temperature dependence of resistivity $\rho(T)$ for $Cd_2Ru_2O_7$ showing three characteristic anomalies around the same temperatures as the $\chi(T)$ curves. Upon cooling down from room temperature, $\rho(T)$ increases gradually and exhibits a broad inflection point around T_0, below which $\rho(T)$ increases in a reduced rate. In light of the broad crossover of $\chi(T)$ around T_0, the decrease of $\rho(T)$ slope might be attributed to the reduced magnetic scattering due to the development of short-range AF correlations. This scenario is consistent with the fact that $\rho(T)$ undergoes a sudden drop at the long-range AF order, changing from the semiconducting-like $d\rho/dT < 0$ at $T > T_N$ to metallic like $d\rho/dT > 0$ at $T < T_N$. The metallic-like state appears in a narrow temperature range and is replaced again by a semiconducting-like dependence at $T < T_{min} \sim T_s$. In light of the μSR measurements [8], the enhanced paramagnetic component below T_s might be responsible for the reentrant semiconducting-like behavior at $T < T_{min}$. Unlike the first-order-like jump of $\chi(T)$, however, $\rho(T)$ changes smoothly around T_{min}. Although $\rho(T)$ seems to have an intimate correlation with the magnetic correlations, the $\rho(T)$ curves measured under $\mu_0 H = 0$ and 7 T overlap in the whole temperature range without discernable magnetoresistance. These results imply that the cubic pyrochlore $Cd_2Ru_2O_7$ is featured by a peculiar electronic band structure that is susceptible to AF order but is hard to alter by a finite magnetic field. In addition, the temperature dependences of $\rho(T)$ in the temperature regions of $T < T_{min}$ and $T > T_N$ do not follow a simple thermal activated behavior, and the magnitude of $\rho(T)$ in the whole temperature range is relatively small, i.e., 3.5–6 mΩ cm, which should fall within the range of bad metal as $Ca_2Ru_2O_7$ [4].

Figure 3(c) displays the specific heat divided by temperature C/T at zero field. A broad λ-type anomaly around T_N provides thermodynamic evidence for the long-range AF order as an intrinsic bulk phase transition rather than from magnetic impurities. However, thermodynamic signatures around T_0 and T_s are absent in the specific heat, which suggests that these transitions are not of a cooperative type. The broad feature in both $\chi(T)$ and $\rho(T)$ around T_0 reflects a gradual crossover, while the reduction of magnetic moment around T_s might not involve changes of the overall magnetic structure. A linear fitting to C/T versus T^2 below 8 K yields a Sommerfeld coefficient $\gamma \approx 7.0(8)\,\text{mJ mol}^{-1}\,\text{K}^{-2}$, in accordance with a metallic ground state with a finite density of states at the Fermi level as reported earlier [23].

The correlated metallic behavior in $Cd_2Ru_2O_7$ is further probed by the thermopower $S(T)$ measurement. As shown in Fig. 3(d), $S(T)$ of $Cd_2Ru_2O_7$ is negative in the whole temperature range, signaling the dominant n-type charge carriers. $|S(T)|$ displays a broad maximum centered around T_0, but it shows no discernable anomaly around T_N and T_s. The latter observations suggest that the changes of scattering rate rather than the density of electronic states at T_N and T_s should play an important role for producing the characteristic anomalies in $\rho(T)$. Since the thermopower is proportional to the energy derivative of $N(E_F)$, the relatively large value of $|S(T)| \sim 100\,\mu\text{V/K}$ at T_0 signals a quite narrow bandwidth in $Cd_2Ru_2O_7$. In contrast to $\rho(T)$, $S(T)$ points to a relatively wide range of metallic behavior, i.e., $d|S|/dT > 0$, at $T < T_0$.

These above characterizations show that the cubic pyrochlore $Cd_2Ru_2O_7$ has a peculiar correlated metallic state that is susceptible to magnetic correlations. The presence of geometrical frustration and strong paramagnetic scattering at $T > T_0$ renders a semiconducting-like behavior in both $\rho(T)$ and $S(T)$, while the development of short-range magnetic correlations below T_0 reduces partially the electron scattering and eventually gives rise to a metalliclike behavior in $\rho(T)$ below T_N upon the formation of long-range AF order. It is the sudden enhancement of the paramagnetic component or the partial reduction of Ru magnetic moments below T_s that causes the reentrant semiconducting-like behavior in $\rho(T)$ below T_{min}. Nevertheless, a considerable $N(E_F)$ is preserved considering the small resistivity, finite γ value, and the metalliclike $S(T)$ in a wide temperature range below T_0. Such an unusual AF metallic ground state is rarely seen among the single-valent transition-metal oxides, and we are thus motivated to investigate its responses to external physical pressure and isovalent chemical substitutions.

B. Effect of high pressure on $Cd_2Ru_2O_7$

Figure 4(a) shows the $\rho(T)$ of $Cd_2Ru_2O_7$ under various hydrostatic pressures up to 1.6 GPa measured with a self-clamped piston cylinder cell (PCC). All $\rho(T)$ curves are insensitive to pressure at $T > T_N$ up to 1.58 GPa and exhibit only a slight reduction in the high-temperature region above T_0. Such a weak response to pressure of $\rho(T)$ at $T > T_N$ is expected considering the small external pressure in comparison with the large bulk modulus of $B_0 = 288$ GPa as determined below. In contrast, $\rho(T)$ below T_N is significantly enhanced upon the application of external pressure, and the resistivity drop in the metalliclike region ($d\rho/dT > 0$) is suppressed quickly accompanied with a slight suppression of T_N. For $P > 0.56$ GPa, no metalliclike region can be observed, and $\rho(T)$ increases quickly upon cooling below T_N following roughly three-dimensional variable range hopping (VRH) conduction [24], i.e., $\rho = \rho_0 \exp(T/T_0)^{-1/4}$, Fig. 4(b); further enhancement of $\rho(T)$ with pressure at $T < T_N$ becomes minute for $P > 1$ GPa. The observed significant enhancement of $\rho(T)$ at $T < T_N$ under such a small external pressure is against our expectation and signals the presence of peculiar electronic

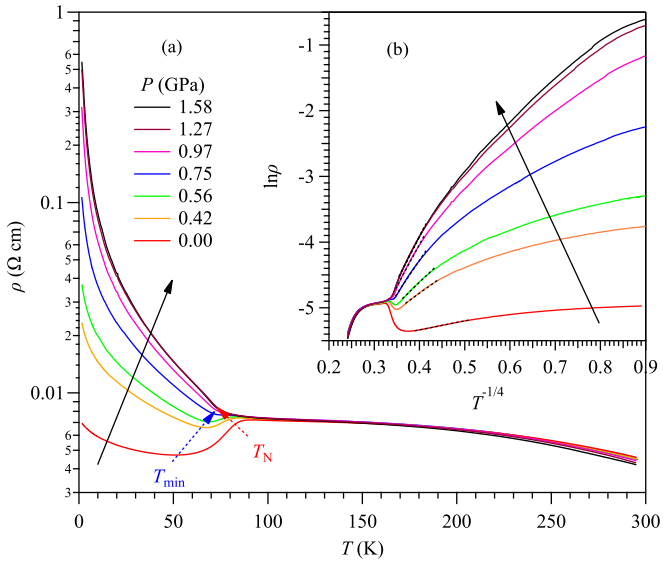

FIG. 4. (a) Resistivity $\rho(T)$ of $Cd_2Ru_2O_7$ under various hydrostatic pressures up to 1.58 GPa measured with a piston cylinder cell. (b) A plot of $\ln\rho$ vs $T^{-1/4}$ for the resistivity data. The broken lines in (b) represent the linear fitting curves below T_N.

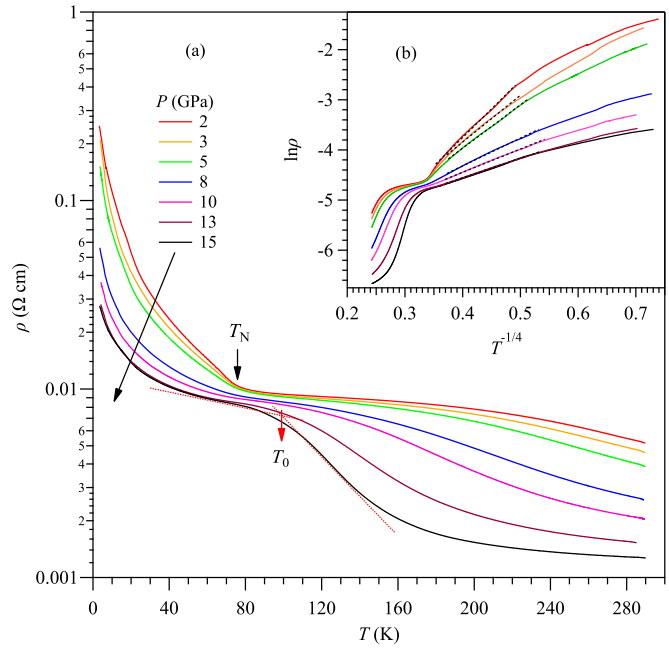

FIG. 5. (a) Resistivity $\rho(T)$ of $Cd_2Ru_2O_7$ under various hydrostatic pressures from 2 to 15 GPa measured with a cubic anvil cell apparatus. (b) A plot of $\ln\rho$ vs $T^{-1/4}$ for the resistivity data. The broken lines represent the linear fitting curves below T_N.

structures below T_N that are susceptible to electron localization under compression. The distinct responses to external pressure of $\rho(T)$ at $T > T_N$ and $T < T_N$ imply that the electronic band structure might undergo a significant reconstruction upon the formation of AF order at T_N, which deserves in-depth studies both experimentally and theoretically.

To probe the electrical transport properties in a wider pressure range, we then measured $\rho(T)$ under various hydrostatic pressures from 2 to 15 GPa by using a cubic anvil cell apparatus. As shown in Fig. 5(a), the $\rho(T)$ curves above 2 GPa also show interesting evolutions. In agreement with the results obtained with PCC, $\rho(T)$ at 2 GPa displays a weak temperature dependence at the high-temperature region with a broad crossover around T_0, followed by a quick enhancement below $T_N \approx 70$ K. With further increasing pressure, $\rho(T)$ at both $T < T_N$ and $T > T_N$ decrease progressively except for the region near T_N, and the plateau region in between T_N and T_0 shrinks gradually. For $P > 8$ GPa, the kink anomaly around T_N can hardly be discerned from $\rho(T)$, and T_0 almost approaches T_N. As a result, the $\rho(T)$ curves at $P \geqslant 10$ GPa are featured by two distinct thermally activated regions. From the VRH plots in Fig. 5(b), it can be seen that pressure reduces the plateau region gradually between T_N and T_0 so that the high-temperature activated region at $T > T_0$ is enlarged and moves closer until it connects smoothly to the low-temperature activation region. Despite the limited temperature range, the activation energy at $T > T_0$ seems to vary only slightly, whereas that at $T < T_N$ decreases progressively with pressure, as seen in Fig. 5(b). It is interesting to note that T_N is insensitive to pressure in such a wide pressure range.

These high-pressure resistivity measurements enable us to uncover unusual responses to pressure of the electronic properties of cubic pyrochlore $Cd_2Ru_2O_7$. Figure 6 summarizes the temperature-pressure phase diagram superimposed by the contour plot of the resistivity curves. As can be seen, the metalliclike region confined in a very narrow temperature range $T_{min} < T < T_N$ is very fragile and is readily replaced by the AF insulating-like state below T_N for $P \geqslant 0.6$ GPa. T_N shows a very weak pressure dependence and seems to merge with T_0 at elevated pressures due to the shrinkage of the plateau region.

To check if these changes of electrical properties under pressure are correlated with some structural transition, we

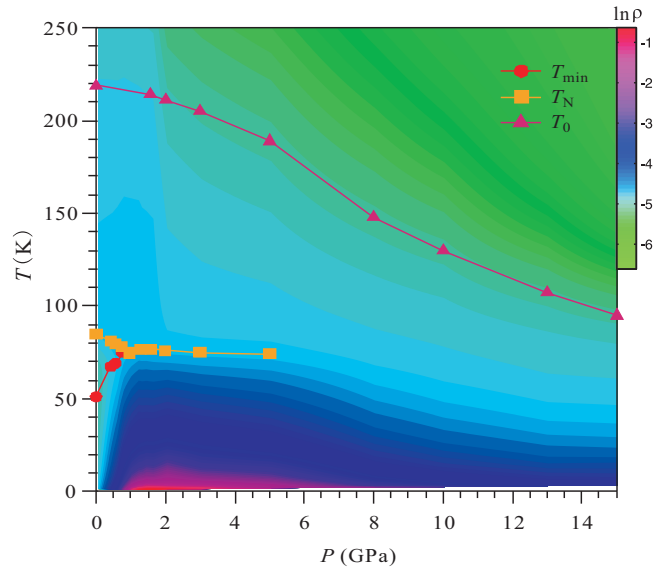

FIG. 6. Temperature-pressure phase diagram of $Cd_2Ru_2O_7$. A contour plot of the resistivity data is superimposed on the phase diagram.

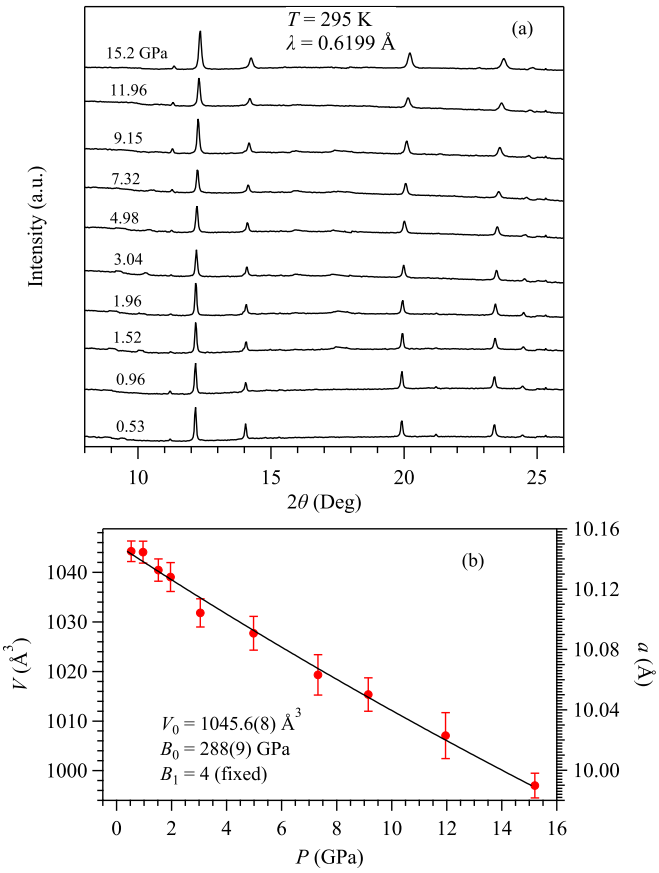

FIG. 7. (a) High-pressure synchrotron XRD patterns of $Cd_2Ru_2O_7$ under various pressures up to 15.2 GPa; (b) Pressure dependence of the lattice constant $a(P)$ and the unit-cell volume $V(P)$. The solid line represents the Birch-Murnaghan fitting to the $V(P)$. The fitting results are given inside the figure.

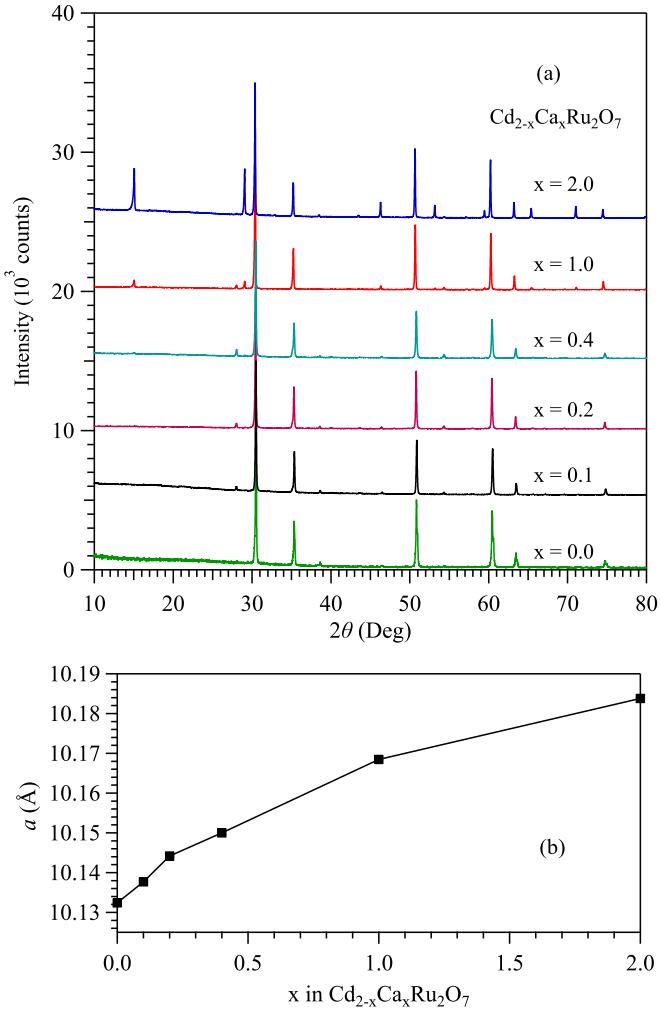

FIG. 8. (a) The XRD patterns of $Cd_{2-x}Ca_xRu_2O_7 (0 \leqslant x \leqslant 2.0)$; (b) the unit-cell parameter a as a function of Ca content x.

performed high-pressure synchrotron XRD on $Cd_2Ru_2O_7$ up to 15.2 GPa at room temperature. As shown in Fig. 7(a), the cubic pyrochlore structure remains stable and no structural phase transformation is observed up to 15.2 GPa. We have fitted the XRD patterns with the LeBail method and plotted the obtained unit-cell constant a and volume V as a function of pressure in Fig. 7(b). The continuous reduction of $V(P)$ can be described well with the Birch-Murnaghan equation, which gives the bulk modulus $B_0 = 288(9)$ GPa and $V_0 = 1045.6(8)$ Å^3 with $B_1 = 4$ fixed. The large bulk modulus indicated that the cubic $Cd_2Ru_2O_7$ is highly incompressible, and thus the dramatic changes of electrical transport properties at $T < T_N$ below 1 GPa have to be associated with some peculiar electronic or magnetic states that are susceptible to change under small lattice compression.

C. Effect of Ca substitution in $Cd_{2-x}Ca_xRu_2O_7$

These unexpected high-pressure effects motivated us to check how the electronic properties of $Cd_2Ru_2O_7$ will evolve under a negative chemical pressure via substituting Ca^{2+} for Cd^{2+} in that the ionic radius of Ca^{2+} (VIII: 1.12 Å) is slightly larger than that of Cd^{2+} (VIII: 1.10 Å) [25]. Figure 8(a) displays the powder XRD patterns of the series of $Cd_{2-x}Ca_xRu_2O_7$ ($x = 0$, 0.1, 0.2, 0.4, 1.0, and 2.0), which are confirmed to form in the cubic pyrochlore structure. On the Ca-rich side, the XRD peaks with odd indices, such as (111) at $\sim 15^\circ$ and (311) at $\sim 29^\circ$, are getting stronger because the difference in scattering factor from the A-site cation and B-site Ru atom becomes bigger. As expected, the lattice constant a increases gradually with x, Fig. 8(b), in accordance with the larger size of Ca^{2+}. Based on the extrapolation of $a(P)$ data shown in Fig. 7(b), substitutions of Ca^{2+} for Cd^{2+} in $Cd_{2-x}Ca_xRu_2O_7$ correspond to the application of negative pressures of -0.5, -1.0, -1.5, -3.0, and -4.3 GPa for $x =$ 0.1, 0.2, 0.4, 1.0, and 2.0, respectively. It should be noted that the obtained $a(x)$ does not follow exactly a linear behavior, or Vegard's law, which is usually preserved only when the bonding character is comparable, e.g., Ca-O versus Sr-O. We believe that the deviation from Vegard's law in the series of $Cd_{2-x}Ca_xRu_2O_7$ is due to the very different bonding nature between Cd-O (with a strong covalent component) and Ca-O (mostly ionic). In this case, the partial substitution of Ca^{2+} for Cd^{2+} not only induces a steric effect, but also leads to additional contraction in Cd-rich samples due to the formation of more covalent bonding.

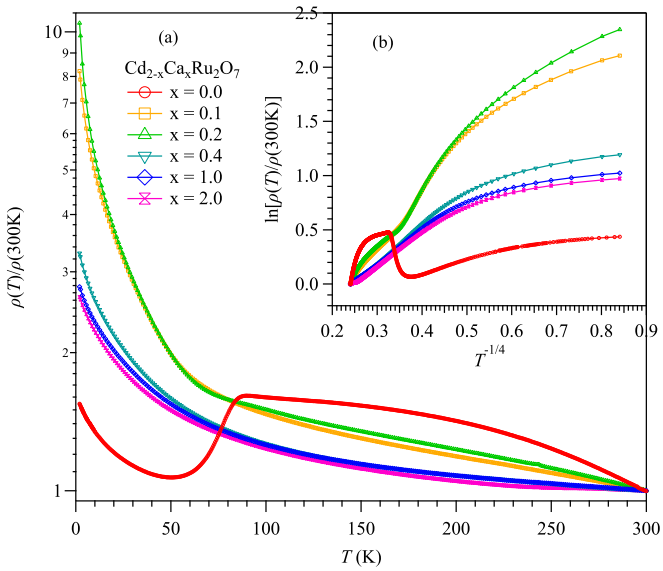

FIG. 9. (a) Temperature dependence of resistivity normalized at 300 K, $\rho(T)/\rho(300\,\mathrm{K})$, for $Cd_{2-x}Ca_xRu_2O_7 (0 \leqslant x \leqslant 2.0)$; (b) a plot of $\ln[\rho(T)/\rho(300\,\mathrm{K})]$ vs $T^{-1/4}$ for the same data.

Figure 9 shows the temperature dependence of resistivity normalized at 300 K, $\rho(T)/\rho(300\,\mathrm{K})$, for the series of $Cd_{2-x}Ca_xRu_2O_7$. Unlike $Cd_2Ru_2O_7$, the isostructural and isoelectronic $Ca_2Ru_2O_7$ is a spin glass with no discernable anomaly in the semiconducting-like $\rho(T)$ around the spin-frozen temperature $T_f \approx 23$ K [4]. As shown in Fig. 9(a), the $\rho(T)$ of $Ca_2Ru_2O_7$ increases upon cooling but does not follow any activated behavior; both the temperature dependence and the magnitude of $\rho(T)$ for our $Ca_2Ru_2O_7$ polycrystalline sample are consistent with those of single crystal reported by Munenaka *et al.* [4]. Interestingly, substitution of only 5–10% Ca for Cd destroys the metallicklike state of $Cd_2Ru_2O_7$ below T_N, and the $\rho(T)$ curves of $x = 0.1$ and 0.2 display a clear reflection point around 60 K followed by a quick increase upon further cooling, reminiscent of the $\rho(T)$ of $Cd_2Ru_2O_7$ at $P \approx 1$ GPa shown in Fig. 4(a). The presence of a gap opening around 60 K for $x = 0.1$ and 0.2 can be seen clearly in the VRH plot shown in Fig. 9(b). The observation of similar behavior in the Ca-doped $Cd_2Ru_2O_7$ with a negative chemical pressure is quite surprising, and further demonstrates the fragile nature of the metallicklike state of $Cd_2Ru_2O_7$ below T_N. Such an unexpected behavior exists in a narrow composition range and disappears upon further Ca doping for $x \geqslant 0.4$. As shown in Fig. 9(a), $\rho(T)$ for $0.4 \leqslant x < 2.0$ exhibits nearly identical behavior to that of $Ca_2Ru_2O_7$ in the whole temperature range.

To check if the gap opening around 60 K for $x = 0.1$ and 0.2 is associated with the formation of magnetic order, we measured the magnetic susceptibility $\chi(T)$ for the series of $Cd_{2-x}Ca_xRu_2O_7$ under $\mu_0 H = 1$ T in both ZFC and FC modes. As shown in Fig. 10(a), a peak anomaly and a splitting of ZFC and FC $\chi(T)$ curves are indeed observed around 40–50 K for $x = 0.1$ and 0.2, signaling the development of AF order or spin freezing. In the paramagnetic region, the $\chi(T)$ curves of $x = 0.1$ and 0.2 display a weak temperature dependence, Fig. 10(b), similar to $Cd_2Ru_2O_7$. Upon further Ca doping, the $\chi(T)$ exhibits a stronger temperature dependence,

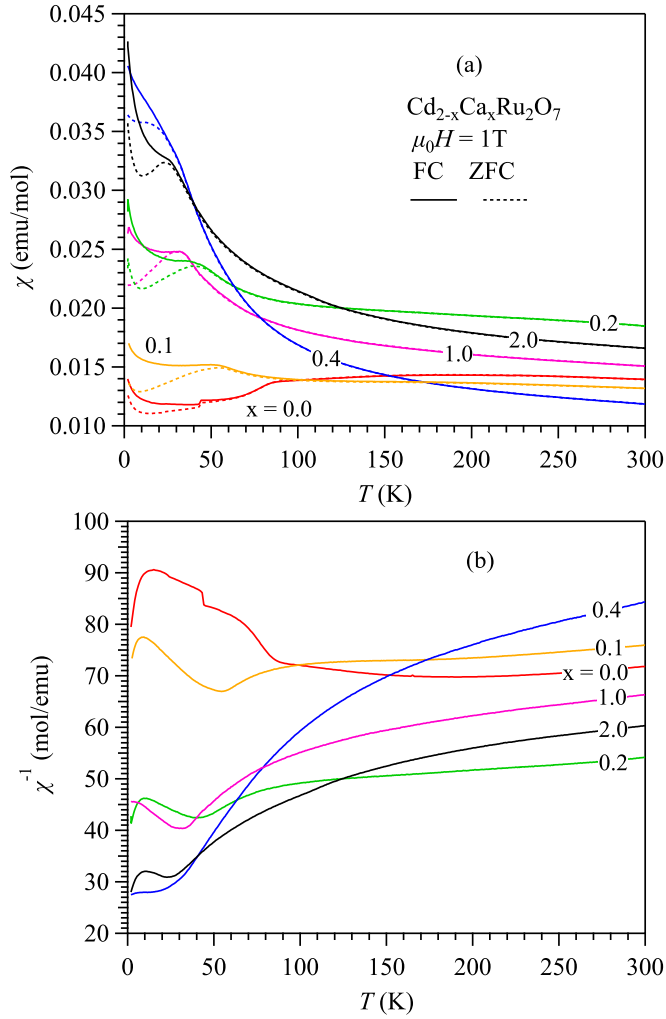

FIG. 10. Temperature dependence of (a) magnetic susceptibility $\chi(T)$ and (b) its inverse $\chi^{-1}(T)$ for the series of $Cd_{2-x}Ca_xRu_2O_7 (0 \leqslant x \leqslant 2.0)$ measured under $\mu_0 H = 1$ T in both zero-field-cooled (ZFC) and field-cooled (FC) modes.

or a larger Curie-Weiss component, which can be seen more clearly in the $\chi^{-1}(T)$ curves of Fig. 10(b). The peak anomaly and the splitting of ZFC and FC curves around 30 K signal the formation of a spin-glass state as in $Ca_2Ru_2O_7$. From these results, we can see that the appearance of an insulating state is accompanied by the development of AF order in $Cd_{2-x}Ca_xRu_2O_7$ ($x = 0.1$ and 0.2).

Figure 11 displays the temperature dependence of thermopower, $S(T)$, for the series of $Cd_{2-x}Ca_xRu_2O_7$ showing dominant n-type charge carriers. Upon Ca doping, the broad maximum at $T_0 \approx 200$ K for $Cd_2Ru_2O_7$ vanishes and the $S(T)$ displays typical metallic behavior. For this isostructural single-valent system, the evolution of $|S|$ at a given temperature reflects the relative change of bandwidth; a broader bandwidth gives a smaller $|S|$. Therefore, the gradual reduction of $|S(T)|$ implies a broadening up of the conduction bands near the Fermi level derived mainly from the hybridized Ru $4d$–O $2p$ orbitals upon Ca doping. This is counterintuitive if one considers only the effect of negative chemical pressure. Instead, the covalency of the A cation (Ca $<$ Cd) has to be invoked because

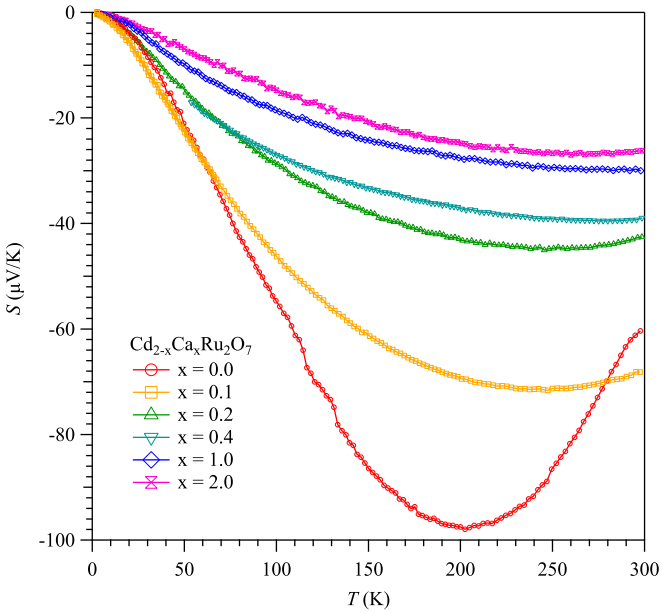

FIG. 11. Temperature dependence of thermopower $S(T)$ for the series of $Cd_{2-x}Ca_xRu_2O_7 (0 \leqslant x \leqslant 2.0)$.

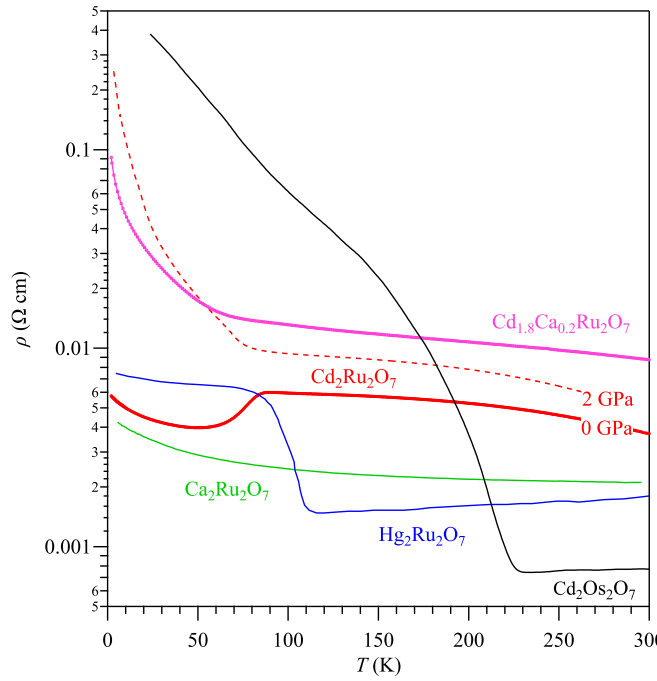

FIG. 12. Comparison of the $\rho(T)$ curves of $Cd_2Ru_2O_7$ at 0 and 2 GPa and that of $Cd_{1.8}Ca_{0.2}Ru_2O_7$ with those of related pyrochlore oxides. The $\rho(T)$ data of $Ca_2Ru_2O_7$, $Hg_2Ru_2O_7$, and $Cd_2Os_2O_7$ are taken from Refs. [4,6,14].

the stronger covalency of Cd with oxygen can effectively reduce the hybridization between Ru $4d$ and O $2p$ orbitals via competing for the O $2p$ orbitals.

D. Discussion

The main finding of the present study is that the AF metalliclike state of $Cd_2Ru_2O_7$ in the temperature range ~40–90 K is very fragile and can be readily converted to an insulating state by applying ~1 GPa hydrostatic pressure or replacing 5–10% Cd with Ca. This finding is unexpected and thus underscores an instability of the electronic states near the localized to itinerant crossover for $Cd_2Ru_2O_7$. It is such an electronic dichotomy that causes the electrical properties to vary sensitively to both internal and external tuning parameters. This can be well illustrated by comparing the resistivity of $Cd_2Ru_2O_7$ with those of related isoelectronic pyrochlore compounds $A_2Ru_2O_7 (A = Ca, Hg)$.

As shown in Fig. 12, the resistivity curves of these Ru^{5+} pyrochlores at ambient pressure differ substantially, which has been ascribed to the different covalency of the nonmagnetic A^{2+} cation as mentioned in the Introduction [8]. The bad metallic behavior observed in $Ca_2Ru_2O_7$ should reflect the intrinsic electronic properties of Ru^{5+} $4d^3$ electrons with dual characters in the presence of strong geometrical frustration. The bandwidth of Ru $4d$–O $2p$ derived bands near the Fermi level are relatively broad in $Ca_2Ru_2O_7$ according to the thermopower results shown in Fig. 11. When Ca^{2+} is replaced by Hg^{2+}, the stronger covalency of Hg^{2+} can effectively reduce the hybridization between the Ru $4d$ and O $2p$ orbitals via competence for the O $2p$ electrons. This will in turn reduce the bandwidth of Ru-O derived bands and strengthen the localized character of Ru $4d$ electrons in accordance with the μSR measurements [8]. As a result, long-range AF order takes place at $T_N = 107$ K accompanied with a sharp metal-to-insulator transition. For the intermediate $Cd_2Ru_2O_7$, the moderate covalency of Cd^{2+} gives rise to electrical properties in between $Ca_2Ru_2O_7$ and $Hg_2Ru_2O_7$. Thus, the diverse electrical properties of $A_2Ru_2O_7$ at ambient pressure should arise from the delicate balance between the itinerant and localized characteristics of the Ru $4d$ electrons tuned by varying the covalency of the A-site cation.

In light of the tunability of Ru $4d$ electrons with dual characters, we can tentatively rationalize the observed AF insulating ground state for $Cd_2Ru_2O_7$ under moderate pressure or a small amount of Ca substitution. For the application of physical pressure, the compressed lattice might first strengthen the Cd-O hybridization so as to enhance the Ru $4d$ localized character, making it closer to $Hg_2Ru_2O_7$ and exhibiting an AF insulating ground state. But the Ru $4d$–O $2p$ derived bands should also broaden up under lattice compression, and such a competing factor is responsible for the reduction of resistivity under higher pressures over 2 GPa, as observed in Fig. 5. In contrast to the application of hydrostatic pressure, the chemical substitutions of Ca^{2+} for Cd^{2+} inevitably introduce lattice disorders, which can usually reduce the Ru-O bandwidth and promote the charge localization. This might be responsible for the initial observation of an AF insulating ground state in $Cd_{2-x}Ca_xRu_2O_7$ ($x = 0.1, 0.2$). But further Ca doping above $x = 0.4$ can overcome this factor and eventually favor a bad metallic behavior as observed in $Ca_2Ru_2O_7$.

As a $5d$-analog of $Cd_2Ru_2O_7$, $Cd_2Os_2O_7$ displays a well-known, continuous metal-to-insulator transition around AF order at $T_N = 225$ K [14] as shown in Fig. 12. It is interesting to note that the resistivity of $Cd_2Ru_2O_7$ at 2 GPa and that of $Cd_{1.8}Ca_{0.2}Ru_2O_7$ resembles that of $Cd_2Os_2O_7$. Following the above-mentioned explanations, the reduction of the Ru-O

bandwidth makes $Cd_2Ru_2O_7$ also similar to $Cd_2Os_2O_7$. This is counterintuitive considering the reduced Coulombic repulsion of 5*d* orbitals with a larger spatial extension. However, the enhanced spin-orbit coupling in the 5*d* compound might renormalize the band structure and lead to narrower bandwidth in comparison with the 4*d* counterpart. This has been well demonstrated in the perovskite iridates [26]. Although the spin-orbit coupling is expected to be reduced considerably in the 4*d* compound, the delicate balance with crystal-field splitting and Hund's coupling might influence the magnetic and transport properties. Thus, further theoretical investigations are needed in order to achieve a comprehensive understanding of these peculiar electronic behaviors near the localized to itinerant crossover.

IV. CONCLUSION

In summary, we have studied the effects of hydrostatic pressure and the isovalent substitution on the electrical transport properties of cubic pyrochlore $Cd_2Ru_2O_7$. Our results demonstrate that its peculiar metalliclike state below AF order at ambient pressure is very fragile and can be readily converted to an insulating state by applying ~1 GPa hydrostatic pressure or replacing 5–10% Cd^{2+} with Ca^{2+}. The resultant resistivity resembles that of 5*d*-analog $Cd_2Os_2O_7$. We have rationalized these unexpected observations in terms of the sensitive tunability of electronic itinerancy/localization dichotomy via side-by-side comparisons with the related compounds $A_2Ru_2O_7$(A = Ca, Hg) and $Cd_2Os_2O_7$. These cubic 4*d*/5*d* pyrochlore oxides offer an important paradigm for studying the exotic physics of correlated electrons on the border of (de)localization in the presence of strong geometrical frustration.

ACKNOWLEDGMENTS

We are grateful to Dr. J.-Q. Yan for helpful discussions. This work is supported by the National Key R&D Program of China (Grants No. 2018YFA0305700 and No. 2018YFA0305800), the National Science Foundation of China (Grant No. 11574377), the Key Research Program of Frontier Sciences and the Strategic Priority Research Program of the Chinese Academy of Sciences (Grants No. QYZDB-SSW-SLH013 and No. XDB07020100). Y.U. is supported by the JSPS KAKENHI (Grant No. 15H03681). J.A.A. acknowledges the financial support of the Spanish MINECO to the project MAT2017-84496-R.

[1] M. Imada, A. Fujimori, and Y. Tokura, Rev. Mod. Phys. **70**, 1039 (1998).
[2] J. B. Goodenough, *Localized to Itinerant Electronic Transition in Perovskite Oxides*, in *Structure and Bonding* (Springer, Berlin, 2001), Vol. 98.
[3] E. Morosan, D. Natelson, A. H. Nevidomskyy, and Q. Si, Ad. Mater. **24**, 4896 (2012).
[4] T. Munenaka and H. Sato, J. Phys. Soc. Jpn. **75**, 103801 (2006).
[5] R. Wang and A. W. Sleight, Mater. Res. Bull. **33**, 1005 (1998).
[6] A. Yamamoto, P. A. Sharma, Y. Okamoto, A. Nakao, H. A. Katori, S. Niitaka, D. Hashizume, and H. Takagi, J. Phys. Soc. Jpn. **76**, 043703 (2007).
[7] W. Klein, R. K. Kremer, and M. Jansen, J. Mater. Chem. **17**, 1356 (2007).
[8] M. Miyazaki, R. Kadono, K. H. Satoh, M. Hiraishi, S. Takeshita, A. Koda, A. Yamamoto, and H. Takagi, Phys. Rev. B **82**, 094413 (2010).
[9] J. S. Gardner, M. J. P. Gingras, and J. E. Greedan, Rev. Mod. Phys. **82**, 53 (2010).
[10] T. Taniguchi, T. Munenaka, and H. Sato, J. Phys.: Conf. Ser. **145**, 012017 (2009).
[11] J. van Duijin, R. Ruiz-Bustos, and A. Daoud-Aladine, Phys. Rev. B **86**, 214111 (2012).
[12] L. Craco, M. S. Laad, S. Leoni, and H. Rosner, Phys. Rev. B **79**, 075125 (2009).
[13] S. Baidya and T. Saha-Dasgupta, Phys. Rev. B **91**, 075123 (2015).
[14] D. Mandrus, J. R. Thompson, R. Gaal, L. Forro, J. C. Bryan, B. C. Chakoumakos, L. M. Woods, B. C. Sales, R. S. Fishman, and V. Keppens, Phys. Rev. B **63**, 195104 (2001).
[15] H. M. Weng, Q. S. Wu, Z. Fang, and X. Dai, APS March meeting, Abstract #C13.011 (2013).
[16] J.-G. Cheng, J.-S. Zhou, and J. B. Goodenough, Phys. Rev. B **81**, 134412 (2010).
[17] Y. Uwatoko, Rev. High Press. Sci. Technol. **12**, 306 (2002).
[18] Y. Uwatoko, K. Matsubayashi, K. Matsubayashi, N. Aso, M. Nishi, T. Fujiwara, M. Hedo, S. Tabata, K. Takagi, M. Tado, and H. Kagi, Rev. High Press. Sci. Technol. **18**, 230 (2008).
[19] J.-G. Cheng, K. Matsubayashi, S. Nagasaki, A. Hisada, T. Hirayama, M. Hedo, H. Kagi, and Y. Uwatoko, Rev. Sci. Instrum. **85**, 093907 (2014).
[20] N. E. Brese and M. O'Keeffe, Acta. Cryst. B **47**, 192 (1991).
[21] I. D. Brown, Z. Kristallogr. **199**, 255 (1992).
[22] A. Krimmel, A. Gunther, W. Kraetschmer, H. Dekinger, N. Buttgen, A. Loidl, S. G. Ebbinghaus, E.-W. Scheidt, and W. Scherer, Phys. Rev. B **78**, 165126 (2008).
[23] K. Blacklock and H. W. White, J. Chem. Phys. **71**, 5287 (1979).
[24] N. F. Mott, Philos. Mag. **19**, 835 (1969).
[25] R. D. Shannon, Acta. Cryst. A **32**, 751 (1976).
[26] B. J. Kim, H. Jin, S. J. Moon, J. Y. Kim, B. G. Park, C. S. Leem, J. Yu, T. W. Noh, C. Kim, S. J. Oh, J. H. Park, V. Durairaj, G. Cao, and E. Rotenberg, Phys. Rev. Lett. **101**, 076402 (2008).